

Topologically induced fractional Hall steps in the integer quantum Hall regime of MoS_2

SK Firoz Islam and Colin Benjamin*

National institute of Science education & Research, Bhubaneswar 751005, India

We study quantum magneto-transport properties of a mono-layer of molybdenum disulfide. Using linear response theory, the effect of topological terms on longitudinal and Hall conductivity is analyzed. The Hall conductivity exhibits fractional steps in the integer quantum Hall regime. Further, complete spin and valley polarization of the longitudinal conductivity is seen in presence of these topological factors. Finally, the Shubnikov de Haas oscillations are suppressed by the inclusion of these topological terms.

I. INTRODUCTION

Molybdenum disulfide (MoS_2) belongs to a new class of 2D materials which have all the advantages of graphene but without its inherent lack of a bandgap and spin-orbit potential, this makes it much more coveted as compared to graphene for possible applications in nanoelectronics and spintronics¹. MoS_2 can be considered to some extent as a semiconductor analog of mono-layer graphene², showing similar phenomena as quantum valley Hall effect³⁻⁵ while it is different from graphene in that spin Hall effect can be seen in addition to quantum valley Hall effect^{4,5}.

Mono-layer MoS_2 is made of a layered structure with covalently bonded sulfur-molybdenum-sulfur atoms in which a single hexagonal layer of molybdenum (Mo) atoms is sliced between two parallel planes of sulfur atoms, each Mo atom co-ordinates with six sulfur (S) atoms in prismatic fashion⁶. Similar to graphene, mono-layer MoS_2 also consists of two valleys K and K' at the corners of its Brillouin zone but with a direct band gap of 1.9 eV⁷.

When few layers of MoS_2 are thinned down to a single layer, the inversion symmetry is broken. This in turn leads to a strong spin-orbit effect⁶, in contrast to mono-layer graphene. The direct band gap and the spin-valley coupling in MoS_2 has made it very convenient for applications in optoelectronics⁸⁻¹¹, valleytronics¹² and spintronics¹³. Recently, several possible applications of mono-layer MoS_2 in valleytronics have been suggested experimentally^{10,11,14}.

Magneto-transport measurements have been one of the best ways to probe electronic systems. In presence of a perpendicular magnetic field applied to the 2D system, energy eigen states become quantized, i.e., form Landau levels. The formation of Landau levels manifests itself through the appearance of quantum oscillation with inverse magnetic field, known as Shubnikov de Haas oscillation. Another unique phenomena related to the perpendicular magnetic field is the quantization of the Hall conductivity, i.e., $\sigma_{xy} = 2(n+1)e^2/h$ with ' n ' an integer and h is the plank constant in conventional 2D system. We use the term conventional for all non-Dirac like electronic systems. This phenomena appears due to the conduction of fermions along the edge boundary caused by the incomplete cyclotron orbits. The longitudinal conductivity (σ_{xx}) becomes completely zero between two consecutive Hall steps.

One of the most well studied non-conventional electronic system is graphene with Dirac like energy-wave vector dispersion. Magneto-transport properties have been studied in graphene,

both theoretically¹⁵⁻¹⁷ as well as experimentally^{18,19}. Later, same has been carried out in silicene^{20,21}, a 2D silicon based hexagonal lattice similar to graphene but without spin and valley degeneracy in presence of gate voltage. Recently, magneto-transport measurements have been performed in MoS_2 ²², where SdH oscillations have been observed. Motivated by this work, in Ref.[23], the first theoretical study of magneto-transport properties of MoS_2 was carried out. Recently, it has been theoretically shown that an electric field normal to MoS_2 can modify the band structure resulting in additional terms in the Hamiltonian which are quadratic in momentum^{24,25}. These terms are also known as topological terms as they can affect the topological features of the system by influencing Berry curvature, Chern number and the Z_2 invariant²⁵. Moreover, these terms have been shown to be tuned by external gate voltage which means that magneto-transport phenomena can be manipulated by gate voltage also²⁵. The magneto-transport properties in presence of scattering mechanism including these topological terms have not been analyzed so far and we rectify this anomaly here.

In this work, we intend to present a theoretical analysis of the consequences of the topological terms in magneto-transport properties of MoS_2 by using linear response theory. We obtain the Landau level energy spectrum and eigen states, and the density of states for different values of the topological parameter. Further, we study the effect of the topological parameter on SdH oscillations and the quantum Hall conductivity. We found that SdH oscillations get suppressed and interestingly fractional Hall steps appear in the quantum Hall conductivity in the integer Hall regime. As an aside, we explore spin and valley polarization of the longitudinal conductivity and find them to be 100% polarized in presence of the topological terms.

This paper is divided into four sections. After giving introduction in section (I), we derive Landau levels and corresponding eigen states in section (II), also discuss density of states here. In section (III), we study longitudinal conductivity and quantum Hall conductivity. Finally, we give our conclusion in section (IV).

II. MODEL HAMILTONIAN AND LANDAU LEVELS

The electronic structure of MoS_2 has been studied with ab initio as well as tight binding calculation^{6,25-27}. We start with a simplified model of low energy effective Hamiltonian⁶:

$$H_0 = \hbar v_F (\tau \sigma_x k_x + \sigma_y k_y) + \frac{\Delta}{2} \sigma_z, \quad (1)$$

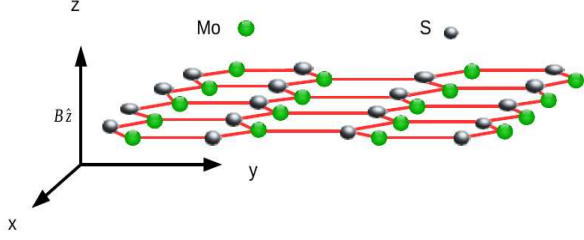


Figure 1. A top view of a mono-layer MoS_2 .

where $v_F = 0.53 \times 10^6$ m/s is the Fermi velocity, $\tau = +(-)$ corresponding to valley K (K'). \mathbf{k} is the 2d momentum, Δ is the direct band gap, σ_i 's are the Pauli matrices with $i = x, y, z$. Similar to the spin, electron in MoS_2 also have another degree of freedom, called sub-lattice. The σ 's of the aforementioned Hamiltonian describe this sublattice parameters.

Spin-orbit interaction and topological parameter:

The removal of inversion symmetry, as mentioned earlier, generates strong spin-orbit interaction which can be included in low energy effective Hamiltonian^{6,28} as $H_{so} = \lambda \tau \frac{\sigma_z - 1}{2} s$ with λ being the strength of spin-orbit interaction and $s = \uparrow (\downarrow)$ describes the real spin of the fermions. As mentioned in introduction, the tight binding calculation based on seven band model have found additional diagonal terms which are quadratic in k but externally tunable by gate voltage in presence of magnetic field²⁵. The gate voltage changes the on site energy of atoms and affects the band gap as well as other parameters. Moreover, these terms can break the valley degeneracy in presence of perpendicular magnetic field²⁵. These additional terms can be included²⁵ as $H_t = (\alpha + \beta \sigma_z) \hbar^2 k^2 / (4m_0)$, where α is constant and β is the topological parameter and m_0 is the free electron mass. Taking all these terms into account, the total low energy effective Hamiltonian can now be expressed as²⁵:

$$H = \hbar v_F (\tau \sigma_x k_x + \sigma_y k_y) + \frac{\Delta}{2} \sigma_z - \tau \frac{\lambda}{2} (1 - \sigma_z) s + \frac{\hbar^2 k^2}{4m_0} (\alpha + \beta \sigma_z). \quad (2)$$

Here, α captures the difference between electron and hole effective masses, given by²⁵ $\alpha = m_0/m_+$, where $m_{\pm} = m_e m_h / (m_h \pm m_e)$ with m_e, m_h the electron and hole effective masses. β depends on electron/hole effective masses as well as on the band gap and spin-orbit interaction strength, given by²⁵ $\beta = m_0/m_- - 4m_0 v_F^2 / (\Delta - \lambda)$.

Inclusion of magnetic field:

When an uniform perpendicular magnetic field is applied to monolayer of MoS_2 , energy of conduction and valence band becomes quantized, i.e., Landau levels are formed without spin and valley degeneracy. Solving the Hamiltonian in presence of the magnetic field, we obtain Landau levels and corresponding eigen states. The magnetic field is included via

Landau-Peirl's substitution: $\mathbf{p} \rightarrow \mathbf{p} + e\mathbf{A}$ in single electron Hamiltonian of mono-layer MoS_2 in the x-y plane as

$$H = v_F \sigma_\tau \cdot \Pi + \frac{\Delta}{2} \sigma_z - \tau \frac{\lambda}{2} (1 - \sigma_z) s + \frac{\Pi^2}{4m_0} (\alpha + \beta \sigma_z), \quad (3)$$

where $\Pi = (\mathbf{p} + e\mathbf{A})$ is 2d momentum operator with e the electronic charge, $\sigma_\tau = (\tau \sigma_x, \sigma_y)$ and \mathbf{A} is the magnetic vector potential, choosing Landau gauge $\mathbf{A} = (0, xB, 0)$ describes the magnetic field $\mathbf{B} = B\hat{z}$.

We introduce dimensionless harmonic oscillator operators $a = \frac{1}{\sqrt{2}}(P_x - iX)$ and $a^\dagger = \frac{1}{\sqrt{2}}(P_x + iX)$, where $X = (x + x_0)/l_c$ with the origin of the cyclotron orbit at $x = -x_0$, where $x_0 = k_y l_c^2$ and $l_c = \sqrt{\hbar/eB}$ -the magnetic length. Also, $P_x = -i\partial/\partial(x/l_c)$ -the dimensionless momentum operator. Then the above Hamiltonian for K-valley ($\tau = +1$) takes the form as

$$H = \begin{bmatrix} \frac{\Delta}{2} + E_{2d}(a^\dagger a + \frac{1}{2})\gamma_+ & \sqrt{2}E_g a \\ \sqrt{2}E_g a^\dagger & -\frac{\Delta}{2} + \lambda s + E_{2d}(a^\dagger a + \frac{1}{2})\gamma_- \end{bmatrix}, \quad (4)$$

where $E_{2d} = \hbar eB/m_0$ and $E_g = \hbar v_F/l_c$, the two energy scales with $l_c = \sqrt{\hbar/eB}$ -magnetic length, and, $\gamma_{\pm} = (\alpha \pm \beta)$. It should be noted that two energy scales arise in the solution of Hamiltonian(4). This is in contrast to the case where the topological parameter is absent²³. The energy scale E_g describes Dirac like dispersion while E_{2d} describes conventional non-Dirac like dispersion. So the influence of the topological parameter is to add conventional 2D electronic features into a Dirac-like system.

To diagonalize the above Hamiltonian, we choose the spinor

$$\Phi(X) = \frac{1}{\sqrt{2}} \sum_j \begin{bmatrix} c_j^+ \\ c_j^- \end{bmatrix} \phi_j(X) \quad (5)$$

as the basis, where $\phi_j(X)$ is harmonic oscillator wave function. Here, $j = 0, 1, 2, 3, \dots$ c_j^{\pm} are the unknown coefficients of upper(+) and lower(-) components spinor. Using this wave function in the eigen value equation $H\Phi = E\Phi$ and multiplying the same harmonic oscillator wave function with different index l , $\phi_l(x)$ from left side, we obtain the following set of coupled equations, after integrating and using orthogonal properties of Hermite polynomials we get

$$[E_{2d}(l + \frac{1}{2})(\alpha + \beta) + \frac{\Delta}{2} - E]c_l^+ + E_g \sqrt{2(l+1)}c_{l+1}^- = 0 \quad (6)$$

and

$$E_g \sqrt{2l}c_{l-1}^+ + [E_{2d}(l + \frac{1}{2})(\alpha - \beta) - \frac{\Delta}{2} + \lambda s - E]c_l^- = 0. \quad (7)$$

In Eq.(6), we make transformation $(l + 1) \rightarrow n$, a new index while in Eq.(7) we keep $l \rightarrow n$. This is the usual way for solving eigen value problem for 2D electronic systems²⁹.

Finally, we have

$$[E_{2d}(n - \frac{1}{2})(\alpha + \beta) + \frac{\Delta}{2} - E]c_{n-1}^+ + E_g \sqrt{2n}c_n^- = 0 \quad (8)$$

and

$$E_g \sqrt{2n}c_{n-1}^+ + [E_{2d}(n + \frac{1}{2})(\alpha - \beta) - \frac{\Delta}{2} + \lambda s - E]c_n^- = 0, \quad (9)$$

here $n = 1, 2, 3, 4, \dots$ are the Landau level index. Similar coupled equations can be obtained for K' -valley too. Solving Eqs. (8-9), we get Landau levels as:

$$E_\xi = \frac{\lambda\tau s}{2} + (\alpha n - \tau \frac{\beta}{2}) E_{2d} + p \sqrt{2nE_g^2 + [\frac{\Delta - \lambda\tau s}{2} + E_{2d}(\beta n - \tau \frac{\alpha}{2})]^2}. \quad (10)$$

Here, $\xi = \{k_y, \zeta\}$ with $\zeta = \{n, s, \tau, p\}$, where $p = +(-)$ stands for conduction (valence) band. Note that in absence of the topological parameter, energy levels of $K_{\uparrow(\downarrow)}$ is equivalent to $K'_{\downarrow(\uparrow)}$ but this symmetry is now broken. The magnetic field dependency of Landau levels can be shown as

$$E_\xi(B) = \frac{\lambda\tau s}{2} + (\alpha n - \tau \frac{\beta}{2}) \frac{\hbar e B}{m_0} + p \sqrt{2n \frac{\hbar^2 v_F^2 e B}{\hbar} + [\frac{\Delta - \lambda\tau s}{2} + \frac{\hbar e B}{m_0}(\beta n - \tau \frac{\alpha}{2})]^2} \quad (11)$$

The ground state energy in K-valley can be obtained from Eq.(7) as $E_{0,+s} = \frac{E_{2d}}{2}(\alpha - \beta) - \frac{\Delta}{2} + \lambda s$. Similarly, for K' -valley which is independent of spin-orbit interaction $E_{0,-} = \frac{E_{2d}}{2}(\alpha + \beta) + \frac{\Delta}{2}$. Note that ground state energy is negative in K-valley while it is positive in K' -valley, as $\Delta/2$ is much higher than E_{2d} and λ . The corresponding wave functions in both valleys are

$$\Phi_\xi(x, y) = \frac{e^{ik_y y}}{\sqrt{L_y}} \begin{bmatrix} \tau A_{n,s}^{\tau,p} \phi_{n-1}[\frac{x+x_0}{l_c}] \\ B_{n,s}^{\tau,p} \phi_n[\frac{x+x_0}{l_c}] \end{bmatrix} \quad (12)$$

with

$$A_{n,s}^{\tau,p} = \frac{E_g \sqrt{2n}}{\sqrt{2nE_g^2 + [E_{2d}(n - \frac{\tau}{2})(\alpha + \beta) + \frac{\Delta}{2} - E_\zeta]^2}} \quad (13)$$

and

$$B_{n,s}^{\tau,p} = \frac{E_\xi - E_{2d}(n - \frac{\tau}{2})(\alpha + \beta) - \frac{\Delta}{2}}{\sqrt{2nE_g^2 + [E_{2d}(n - \frac{\tau}{2})(\alpha + \beta) + \frac{\Delta}{2} - E_\zeta]^2}}. \quad (14)$$

Here, $e^{ik_y y} / \sqrt{L_y}$ is the normalization factor. $\phi_n(X) = \frac{1}{\sqrt{2^n n! l_c \sqrt{\pi}}} e^{-X^2/2} H_n(X)$ is the harmonic oscillator wave function with $H_n(X)$ the Hermite polynomial of order n . The harmonic oscillator wave functions $\phi_{n-1}(x)$ and $\phi_n(x)$ are interchanged in K' -valley. The ground state wave function in K-valley is

$$\Phi_{k_y, 0, +}(x, y) = \frac{e^{ik_y y}}{\sqrt{L_y}} \begin{bmatrix} 0 \\ \phi_0(x) \end{bmatrix} \quad (15)$$

and in K' -valley is

$$\Phi_{k_y, 0, -}(x, y) = \frac{e^{ik_y y}}{\sqrt{L_y}} \begin{bmatrix} \phi_0(x) \\ 0 \end{bmatrix}. \quad (16)$$

We plot the spin and valley dependent Landau levels in Fig-

ure. (2a). we see that Landau levels in the conduction band linearly increases with magnetic field, while in the valence band they linearly decrease with the magnetic field.

Landau levels have two magnetic field dependent energy scales, one is topologically induced $E_{2d} \propto B$ and the Dirac nature induced $E_g \propto \sqrt{B}$, which compete with each other. Now we only discuss conduction band Landau levels only, as we consider Fermi level lies in the conduction band.

Landau levels are always well separated in valley space but not so in spin space. In fact for smaller indices's, the spin splitting is unobservable. In absence of the topological parameter, spin splitting would be same in both valleys but opposite i.e., energy levels corresponding to K_{\uparrow} (K_{\downarrow}) is equivalent to K'_{\downarrow} (K'_{\uparrow}), thus each Landau level is still doubly degenerate. The topological parameter is intrinsically associated with the Landau level index as shown in En.(10), see the second term under the square root the topological factor β is multiplied with n which is in complete contrast to the valley dependent zeeman effect as treated in Ref.[23]. At strong magnetic field, the effect of the topological parameter is expected to be dominant over Dirac kinetic energy terms. In the valence band (lower panel of Figure (2a), spin splitting is very strong in both valleys. We also see a fascinating phenomena of vanishing Landau level spin splitting in valley space, see for example the Landau level index $n = 10$ where $E_{10}(K_{\downarrow}) \cong E_{10}(K'_{\downarrow})$, indicated by 1X. For higher Landau levels again, we see a similar thing but now not in the same level but between adjacent Landau levels see the point marked 2X in figure (2b) i.e., $E_{11}(K_{\downarrow}) \cong E_{12}(K'_{\downarrow})$. To conclude, we see that intra and inter valley and spin dependent Landau level gaps may disappear as a consequence of topological parameter. This has major consequence for SdH oscillations and quantum Hall conductivity as we describe in the next section, but before that we now concentrate on the density of states.

Density of states

The density of states (DOS) in presence of perpendicular magnetic field would be a series of delta function because of the discrete energy spectrum expressed as

$$D(E) = g_s g_v \sum_{k_y, \zeta} \delta[E - E_{k_y, \zeta}], \quad (17)$$

where, g_s and g_v are spin and valley degeneracy, respectively. The summation over k_y can be evaluated from the fact that origin of the cyclotron orbit is limited by the system dimensions i.e., $0 \leq |x_0| \leq L_x$, or $0 \leq k_y \leq L_x/l_c^2$, thus

$$\sum_{k_y} \rightarrow \frac{L_y}{2\pi} \int_0^{L_x/l_c^2} dk_y = \frac{\Omega}{2\pi l_c^2}, \quad (18)$$

with $\Omega = L_x L_y$. Here, the factor $L_y/(2\pi)$ appears from the boundary condition. Now the DOS per unit area can be expressed as

$$D(E) = C_0 \sum_{\zeta} \delta[E - E_{\zeta}], \quad (19)$$

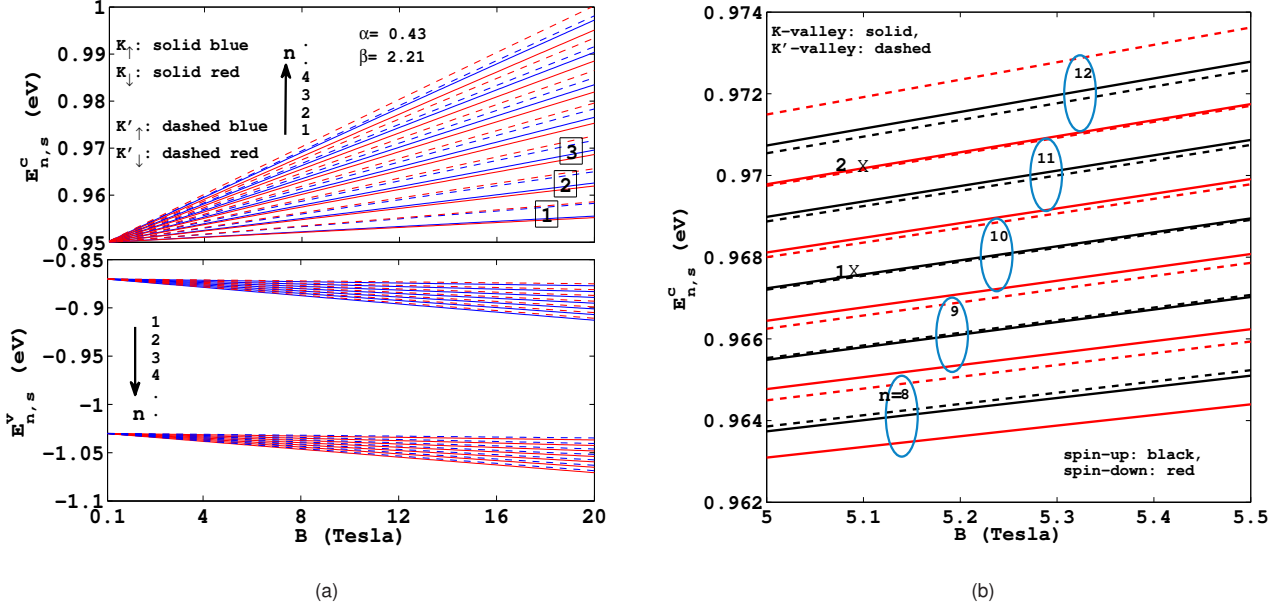


Figure 2. plots of Landau levels in both valley and in conduction (upper panel) and valence (lower panel) band in left figure. The right figure shows the zoomed part of few Landau levels between $B = 5$ to 5.5 T. Following parameters are used : $v_F = 0.53 \times 10^5$ m/s, direct band gap $\Delta = 1.9$ eV and spin-orbit interaction strength $\lambda = 0.08$ eV.

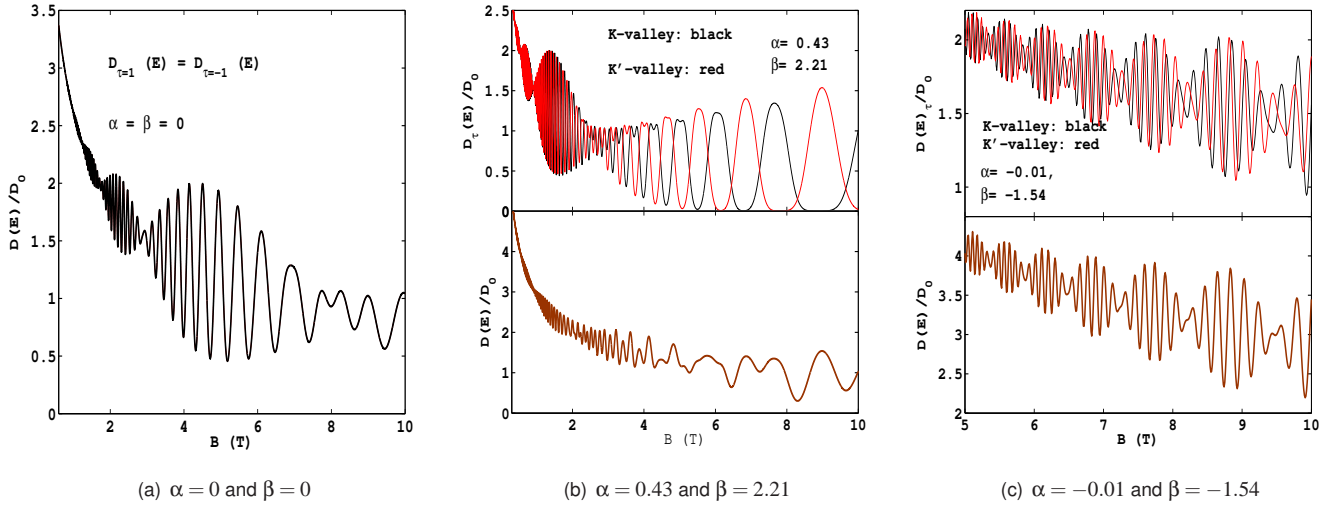


Figure 3. Plots of density of states in conduction band versus magnetic field without (a) and with (b and c) topology parameters at Fermi energy $E_f = 0.96$ eV.

where $C_0 = g_s g_v / (2\pi l_c^2)$ with $g_s = g_v = 1$ as there is no spin and valley degeneracy. To plot DOS, we shall use the Gaussian distribution of the delta function as

$$D(E) = D_0 \sum_{\zeta} \exp\left[-\frac{(E - E_{\zeta})^2}{2\Gamma^2}\right], \quad (20)$$

where $D_0 = C_0 / \sqrt{2\pi}\Gamma$ with the width of the Gaussian distribution $\Gamma = 0.1 \sqrt{B}$ meV³⁰. DOS become oscillatory in presence of magnetic field due to the quantization of energy spectrum,

see Figure (3). In absence of the topological parameter, both K and K'-valleys produce beating pattern in DOS oscillations with beating nodes at the same location. This is expected since the degeneracy $E_K^{\uparrow(\downarrow)} \cong E_{K'}^{\downarrow(\uparrow)}$. The total DOS without topological parameter is shown in Figure(3a). Beating pattern is caused by the superposition of two closely separated frequencies of DOS for spin-up and down branches. Figure(3b) and (3c) show the effects of inclusion of topological parameters. Figure(3b) shows that though beating pattern appears in two valleys individually but there is a definite phase difference

between two valleys which resulted in suppression of the total DOS oscillation (lower panel) for $\alpha = 0.49$ and $\beta = 2.21$. But this is not followed when $\beta = -1.54$ in Figure(3c), where the phase difference between two valleys is small, and sustains DOS oscillation in total DOS (lower panel) with spin-split induced beating pattern.

III. ELECTRICAL CONDUCTIVITY

At low temperature regime, there are mainly two kind of mechanisms by which electronic conduction takes place. One is due to the scattering of cyclotron orbits from localized charged impurities- the collisional contribution to the conductivity. The other contribution is the diffusive conductivity which depends on the drift velocity of the electron³¹. Since drift velocity $v_i = \hbar^{-1} \partial E / \partial k_i = 0$ in our case with $i = x, y$, therefore diffusive contribution to the conductivity vanishes. To calculate different components of conductivity tensor (Hall conductivity- σ_{xy} and the longitudinal conductivity - $\sigma_{xx/y}$), we shall use linear response theory modified in Ref.[32].

Longitudinal conductivity:

Here, we assume that electrons are scattered elastically by randomly distributed charged impurities. This types of scattering is important at low temperature. The expression for longitudinal conductivity is given by³²

$$\sigma_{xx} = \frac{\beta_T e^2}{2\Omega} \sum_{\xi, \xi'} f_{\xi} (1 - f_{\xi'}) W_{\xi, \xi'} (x_{\xi} - x_{\xi'})^2. \quad (21)$$

Here, $\beta_T = (k_B T)^{-1}$, $f_{\xi} = [1 + \exp\{\beta_T (E_{\xi} - E_F)\}]^{-1}$ is the Fermi-Dirac distribution function. $x_{\xi} = \langle \xi | x | \xi \rangle$, is the expectation value of the x-component of the position operator when electron is in state $|\xi\rangle$. It can be easily shown that $x_{\xi} = x_0 = k_y l_c^2$, $(x_{\xi} - x_{\xi'})^2 = (q_y l_c^2)^2$ with $k'_y - k_y = q_y$. The scattering rate is given by³²

$$W_{\xi, \xi'} = \frac{2\pi N_I}{\Omega \hbar} \sum_q |U_q|^2 |F_{\xi, \xi'}(\gamma)|^2 \delta(E_{\xi} - E_{\xi'}) \delta_{k_y, k'_y + q_y}. \quad (22)$$

Here, N_I is the impurity density and $\gamma = q^2 l_c^2 / 2$. The 2D Fourier transformation of the screened charged impurity potential $U(r) = e^{-k_0 r} / 4\pi \epsilon_0 \epsilon_r r$ is $U_q = U_0 [q^2 + k_0^2]^{-1/2} \simeq U_0 / k_0$ for short range delta function-like potential, where $U_0 = e^2 / 4\pi \epsilon_0 \epsilon_r$; k_0 is the screening vector. And the form factor $F_{\xi, \xi'}(\gamma) = \langle \xi | e^{i\vec{q} \cdot \vec{r}} | \xi' \rangle$ which can be evaluated for elastic scattering, the dominant contribution, i.e., $n = n'$ as

$$|F_{n, n}(\gamma)|^2 = e^{-\gamma} [|A_{n, s}^{\tau, p}|^2 L_n(\gamma) + |B_{n, s}^{\tau, p}|^2 L_{n-1}(\gamma)]^2. \quad (23)$$

Here, $L_n(\gamma)$ is the Laguerre polynomial of order n . To proceed further, we replace summation over k_y by $\Omega / (2\pi l_c^2)$, $\sum_q \rightarrow \frac{\Omega}{(2\pi)^2} \int q d q d \phi$ and $(x_{\xi} - x_{\xi'})^2 = q_y^2 l_c^4 = [q \sin \phi]^2 l_c^4$, we obtain

$$\sigma_{xx} \simeq \frac{e^2}{h} \frac{N_I U_0^2}{l_c^2 k_0^2 k_B T} \sum_{n, \tau, s, p} G_{\tau, s} I_{n, s}^{\tau, p} f_n^{\tau, s} (1 - f_n^{\tau, s}) \quad (24)$$

where $I_{n, s}^{\tau, p} = |A_{n, s}^{\tau, p}|^4 (2n + 1) + |B_{n, s}^{\tau, p}|^4 (2n - 1) - 2n |A_{n, s}^{\tau, p}|^2 |B_{n, s}^{\tau, p}|^2$ with $A_{n, s}^{\tau, p}$ and $B_{n, s}^{\tau, p}$ are given in Eqs(13) and (14). Also,

$G_{\tau, s} = \Delta_{\tau, s} / (E_g^2 + \Delta_{\tau, s} E_{2d} (\alpha + \beta))$. To obtain $I_{n, s}^{\tau, p}$, the following standard integration result has been used:

$$\int_0^{\infty} \gamma e^{-\gamma} [L_n(\gamma)]^2 d\gamma = (2n + 1). \quad (25)$$

Because of the large momentum separation between two valleys, inter-valley scattering is negligibly small. Spin and valley polarization for longitudinal conductivity can be defined as

$$P_s = \frac{\sigma_{K'}^{\uparrow} - \sigma_{K'}^{\downarrow} + \sigma_{K'}^{\uparrow} - \sigma_{K'}^{\downarrow}}{\sigma_{K'}^{\uparrow} + \sigma_{K'}^{\downarrow} + \sigma_{K'}^{\uparrow} + \sigma_{K'}^{\downarrow}} \quad (26)$$

and

$$P_v = \frac{\sigma_K^{\uparrow} - \sigma_{K'}^{\uparrow} + \sigma_K^{\downarrow} - \sigma_{K'}^{\downarrow}}{\sigma_K^{\uparrow} + \sigma_K^{\downarrow} + \sigma_{K'}^{\uparrow} + \sigma_{K'}^{\downarrow}}. \quad (27)$$

Quantum Hall conductivity:

In linear response regime, the quantum Hall conductivity (σ_{xy}) is defined as³²:

$$\sigma_{xy} = \frac{ie\hbar^2}{\Omega} \sum_{\xi \neq \xi'} [f(E_{\xi}) - f(E_{\xi'})] \frac{\langle \xi | \hat{v}_x | \xi' \rangle \langle \xi' | \hat{v}_y | \xi \rangle}{(E_{\xi} - E_{\xi'})^2}. \quad (28)$$

In the above expression, velocity operators are defined as: $\hat{v}_x = \partial H / \partial p_x$ and $\hat{v}_y = \partial H / \partial p_y$. It is to be noted that here in (28), the matrix elements of velocity operators appear which is in general non-zero (see the appendix) unlike the drift velocity element defined earlier which for our case is zero. After performing summation over k_y , the above expression simplifies to

$$\sigma_{xy} = \frac{ie^2 \hbar}{2\pi^2 l_c^2} \sum_{\zeta \neq \zeta'} [f(E_{\zeta}) - f(E_{\zeta'})] \frac{\langle \zeta | \hat{v}_x | \zeta' \rangle \langle \zeta' | \hat{v}_y | \zeta \rangle}{(E_{\zeta} - E_{\zeta'})^2} \quad (29)$$

Note that $\zeta = \{n, s, \tau, p\}$. The velocity operators are obtained as

$$\hat{v}_x = (\alpha + \beta \sigma_z) \frac{p_x}{2m_0} + \tau v_F \sigma_x \quad (30)$$

and

$$\hat{v}_y = (\alpha + \beta \sigma_z) \frac{p_y + eBx}{2m_0} + v_F \sigma_y \quad (31)$$

Now, as usual the zero level ($n = 0$) contribution to the Hall conductivity has to be treated separately as

$$\begin{aligned} \sigma_{xy}^{0, \tau} &= \frac{ie^2 \hbar}{2\pi^2 l_c^2} \sum_{n', s, p, p'} [f(E_{0, s}^{\tau, p}) - f(E_{n', s}^{\tau, p'})] \\ &\times \frac{\langle 0, s, \tau, p | \hat{v}_x | n', s, \tau, p' \rangle \langle n', s, \tau, p' | \hat{v}_y | 0, s, \tau, p \rangle}{(E_{0, s}^{\tau, p} - E_{n', s}^{\tau, p'})^2}. \end{aligned} \quad (32)$$

Details of the calculation of the expectation values of velocity operators are given in appendix.

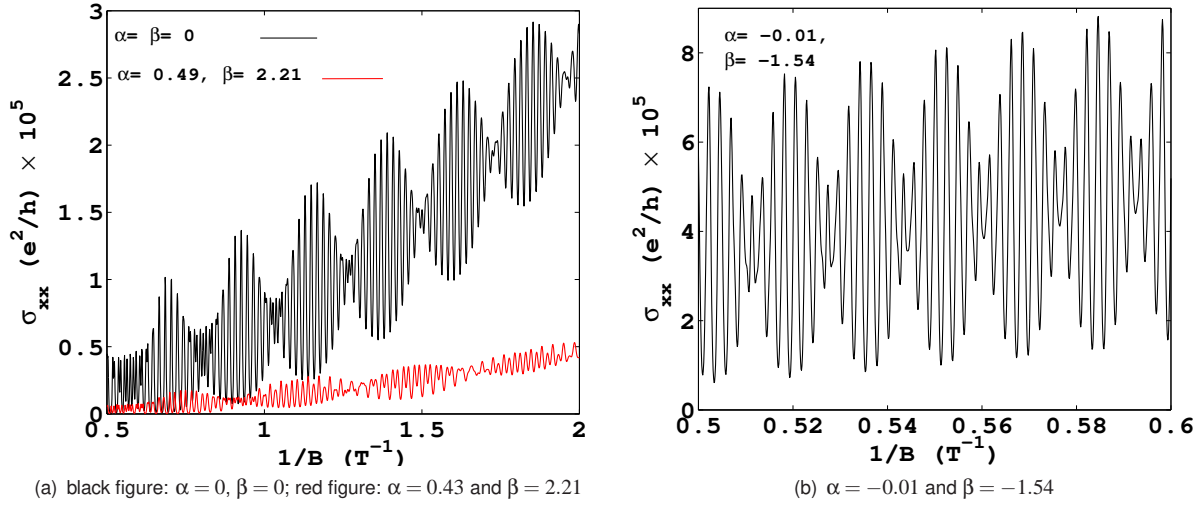


Figure 4. Plots of the longitudinal conductivity versus inverse magnetic field.

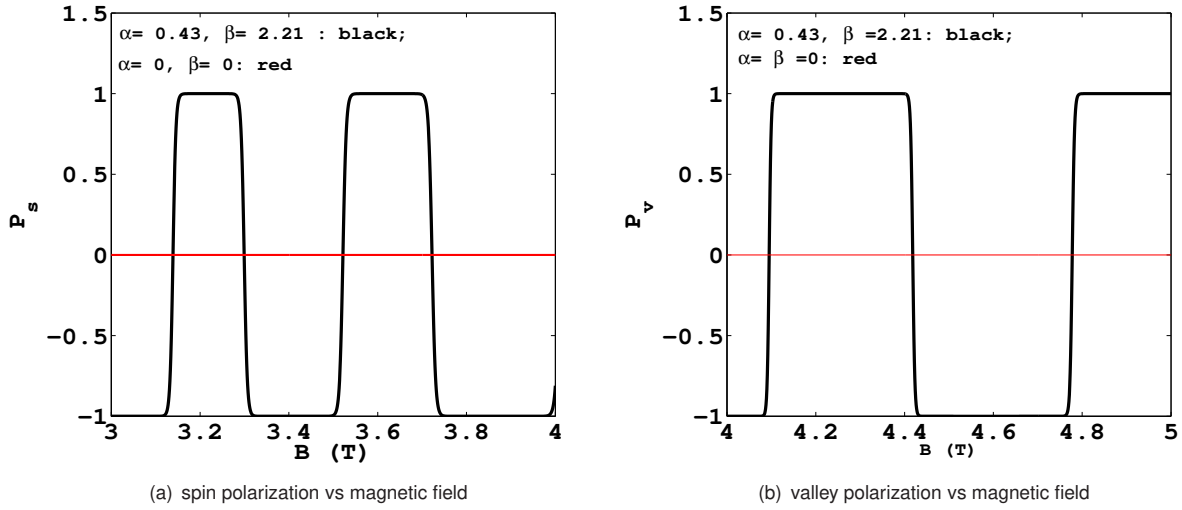


Figure 5. Plots of the spin/valley polarization in longitudinal conductivity versus magnetic field.

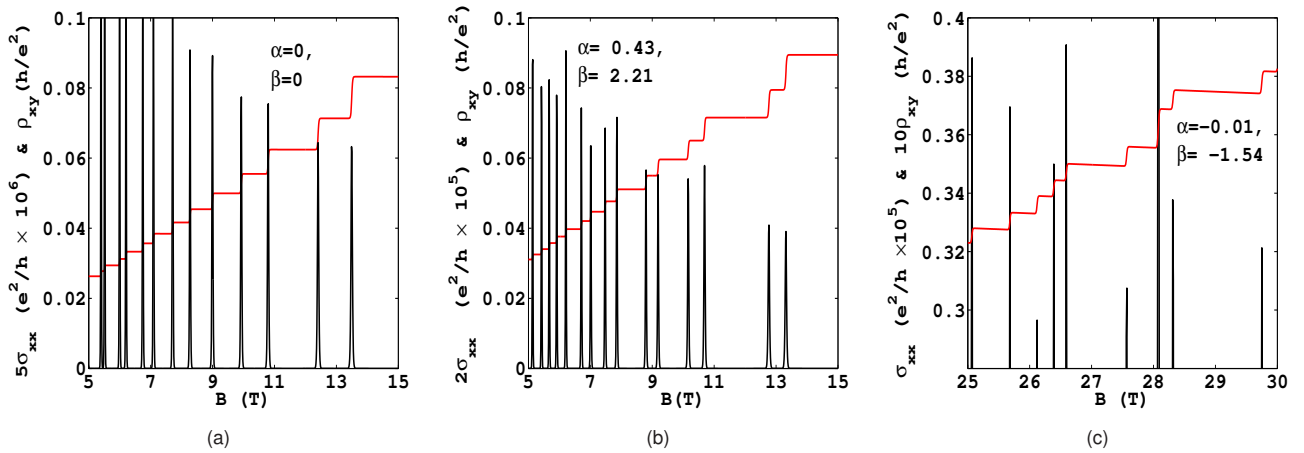
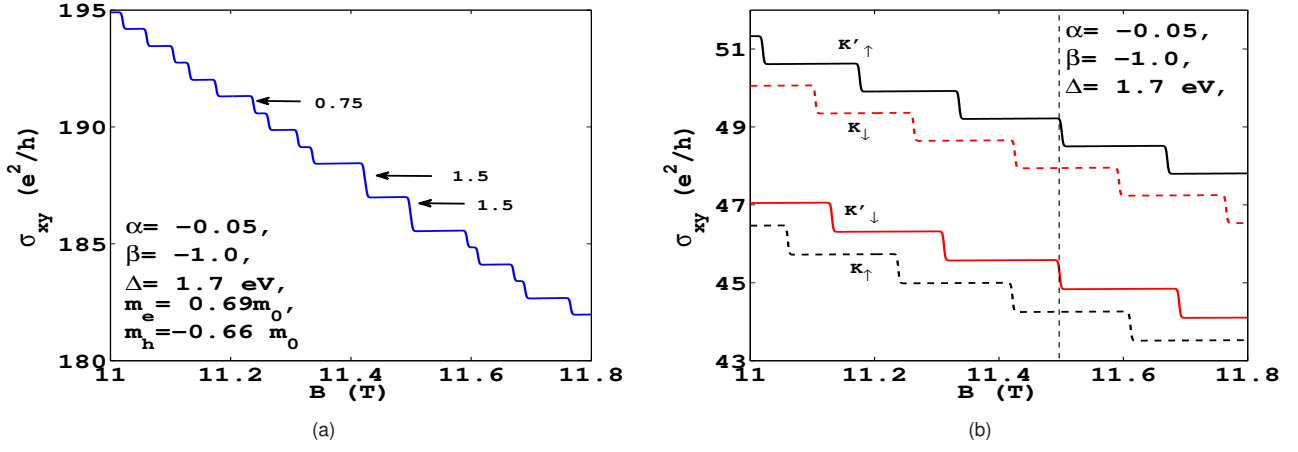
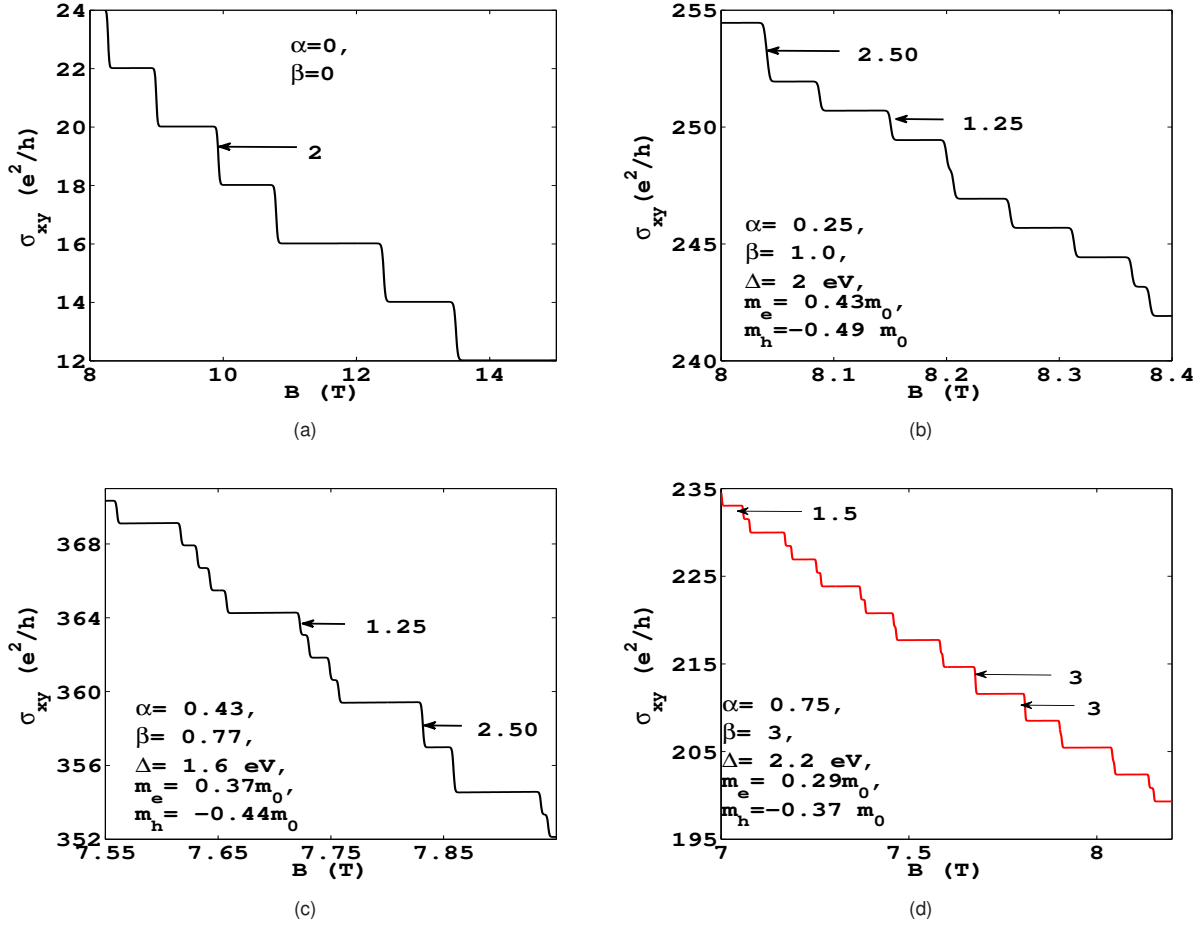


Figure 6. Longitudinal conductivity (black) and Hall resistivity (red) versus magnetic field (B) for different values of α and β .


 Figure 7. Hall conductivity versus magnetic field (in Tesla) for different values of α and β .

 Figure 8. Hall conductivity versus magnetic field (in Tesla) for different values of α and β .

IV. RESULTS AND DISCUSSION

For numerical plots of longitudinal conductivity and Hall conductivity, we use the following parameters: Fermi level is at

$E_F = 0.96$ eV in the conduction band. As gate voltage can tune the band gap, we choose three sets of parameters^{24,25}: $\alpha = 0.43$ and $\beta = 2.21$ corresponding to $\Delta = 1.9$ eV, $\lambda = 0.08$ eV, effective mass of electron $m_e = 0.37m_0$ and hole $m_h = -0.44m_0$; $\alpha = -0.01$ and $\beta = -1.54$ corresponding to $\Delta =$

1.83 eV, $\lambda = 0.08$ eV, effective mass of electron $m_e = 0.95m_0$ and hole $m_h = -0.94m_0$. Temperature (T) = 0.3 K, impurity density (N_I) = $10^{13}m^{-2}$, screening wave vector: $k_0 = 10^7m^{-1}$, relative permittivity of MoS_2 : $\epsilon_r = 7.3^{22,33}$.

In Figure (4), we plot longitudinal conductivity (σ_{xx}) versus inverse magnetic field ($1/B$) by using Eq.(24), to observe SdH oscillations. Figure(4a) contains two plots, black is for $\alpha = \beta = 0$ and red is for non-zero and $\alpha = 0.43$ and $\beta = 2.21$. The black and red plots show appearance of beating pattern in SdH oscillations. However, the number of beating nodes decreases and oscillations amplitude is damped because of the topological parameter ($\beta = 2.21$). The appearance of SdH oscillations in longitudinal conductivity is the direct consequence of oscillations in DOS. Total longitudinal conductivity produces beating pattern in SdH oscillation because of the small difference in frequencies of each spin branch, see En. (10) where $s = \uparrow, \downarrow$ makes a significance difference in the energy. The beating pattern does not depend on topological parameter ' β '. However ' β ' can influence the number of beating nodes, this is because of the association of Landau level index ' n ' with β in energy spectrum (see Eq.(10)). The origin of the damping in SdH oscillations can be traced to the behavior of DOS, as shown in Figure(3b), which shows two valleys in almost opposite phase because of ' β '. SdH oscillations for negative value of topological parameter $\beta = -1.54$ and $\alpha = -0.01$ is shown in Figure(4b), where the number of beating nodes increases within a small range of inverse magnetic field. This is because the Landau levels spacing has become more smaller, as a result within small range of magnetic field many Landau levels can pass through Fermi level and thus increase the frequency of the SdH oscillations.

Next we plot spin and valley polarization in longitudinal conductivity versus magnetic field in Figure (5a,b). We find that 100% spin polarization can be achieved for finite value of topological parameter as shown by black solid line. In absence of topological parameter, there is no spin polarization as shown by red solid line. In Figure(5b), we show fully valley polarization can also be achieved.

Quantum Hall resistivity ($\rho_{xy} = 1/\sigma_{xy}$) and longitudinal conductivity are plotted versus magnetic field in Figure(6) by using the formula(28) and (24). Without topological parameter, plateaus and steps are increasing slowly with magnetic field in Hall resistivity and sharp peaks of longitudinal conductivity arise at each step of the Hall resistivity as shown in Figure(6a). The longitudinal conductivity shows peaks at each step of the Hall resistivity, as shown in Figure (6), corresponding to passing of Landau levels through Fermi energy.

When $\alpha = 0.49$ and $\beta = 2.21$, We observe that behavior of steps remain unchanged but longitudinal conductivity peaks appear in pairs, two nearest pairs are well separated because of the topological parameter induced valley separation. These SdH peaks appearing in pairs actually correspond to spin-splitting of Landau levels. Small plateaus arise between spin-split conductivity peaks while longer plateaus arise between two nearest pairs as shown in Figure (6b).

In the Figure(6c), we plot the same for $\alpha = -0.01$ and $\beta = -1.54$, where we see that plateaus are random in size and a big step arises around $B = 28T$. Here, we have shifted the x-

axis for better visualization, as step size becomes too small to be observed properly.

To understand the origin of big steps, we plot Hall conductivity versus magnetic field for different sets of parameters in Figure(7). In Figure(7a), we found that steps are not fixed in size i.e., there are two different size of steps: $n_{eff}(e^2/h)$ and $(n_{eff}/2)(e^2/h)$ with $n_{eff} = 1.5$, indicated by black arrow. The value of n_{eff} is obtained from numerical datas of Hall conductivity. The origin of big steps can be explained from Figure(7b) where each spin component in each valley is plotted separately. It shows that big step arises when spin-up and down components of Hall conductivity of K/K' -valley exhibit a step at the same magnetic field, as shown by a vertical dashed line. This phenomena is the consequence of vanishing spin-splitting Landau level in valley space, as discussed in the Landau level plot (see Figure(2b)). For $\alpha = \beta = 0$, steps are always $2(e^2/h)$ including spin-splitting as shown in Figure(8a). The enhancement of the quantum Hall conductivity can be traced to the α, β dependent additional terms which appear in the velocity matrix elements. Similar patterns are observed for other two sets of parameters (given in the figures) in Figure(8b and 8c). In Figure (8b), steps are found as $2.5(e^2/h)$ and $1.25(e^2/h)$; same steps appear in Figure (8c). It should be noted that in all these figures, Hall conductivity steps are always of two types, n_{eff} and $n_{eff}/2$ where n_{eff} is the traditional integer quantum Hall step while the $n_{eff}/2$ is the topologically induced fractional step.

V. CONCLUSION

We have studied quantum magneto-transport properties of mono-layer MoS_2 including the gate voltage controlled topological parameters, α, β . We found that magneto-conductivity oscillations are strongly affected by these topological parameters. Moreover, when topological parameters are positive there is a suppression of SdH oscillation because of the almost opposite phase between the oscillations arising from two valleys. When topological parameters are negative, this effect is much stronger which causes large number of beating pattern within a small range of magnetic field. The topological parameters ' β ' also causes a complete separation between two valleys, as a result we get fully spin and valley polarized magneto-conductivity. In integer quantum Hall regime, we see in addition to the usual integer steps, fractional steps of the Hall conductivity. The present study will be extended in future to understand theoretically the effects of gate voltage controlled topological factors on magneto-thermal properties.

VI. ACKNOWLEDGEMENT

This work is financially supported by the Department of Science and Technology (Nano- mission), Govt. of India for funds under Grant No. SR/NM/NS-1101/2011.

VII. APPENDIX

The velocity matrix elements are calculated for K-valley ($\tau = +$) and $n \geq 1$ as:

$$\begin{aligned} & \langle n, s, +, p | \hat{v}_x | n', s, +, p' \rangle \\ &= (\alpha + \beta) v_0 A_{n,s}^{+,p} A_{n',s}^{+,p'} [\sqrt{n'} \delta_{n-1,n'} + \sqrt{n'-1} \delta_{n-1,n'-2}] \\ &+ v_F [A_{n,s}^{+,p} B_{n',s}^{+,p'} \delta_{n-1,n'} + A_{n',s}^{+,p'} B_{n,s}^{+,p} \delta_{n,n'-1}] \\ &+ v_0 (\alpha - \beta) B_{n,s}^{+,p} B_{n',s}^{+,p'} [\sqrt{n'+1} \delta_{n,n'+1} + \sqrt{n'} \delta_{n,n'-1}], \end{aligned} \quad (33)$$

where $v_0 = \sqrt{\hbar \omega_c / 8m_0}$. Similarly for K'-valley ($\tau = -$) and $n \geq 1$

$$\begin{aligned} & \langle n, s, -, p | \hat{v}_x | n', s, -, p' \rangle \\ &= (\alpha + \beta) v_0 A_{n,s}^{-,p} A_{n',s}^{-,p'} [\sqrt{n'+1} \delta_{n,n'+1} + \sqrt{n'} \delta_{n,n'-1}] \\ &- v_F [A_{n',s}^{-,p} B_{n,s}^{-,p'} \delta_{n,n'-1} + A_{n,s}^{-,p'} B_{n',s}^{-,p} \delta_{n',n-1}] \\ &+ v_0 (\alpha - \beta) B_{n,s}^{-,p} B_{n',s}^{-,p'} [\sqrt{n'} \delta_{n-1,n'} + \sqrt{n'-1} \delta_{n-1,n'-2}]. \end{aligned} \quad (34)$$

The matrix elements of \hat{v}_y are evaluated for $\tau = +1$ and $n \geq 1$ as

$$\begin{aligned} & \langle n', s, +, p | \hat{v}_y | n, s, +, p' \rangle \\ &= (-i) \left[(\alpha + \beta) v_0 A_{n,s}^{+,p} A_{n',s}^{+,p'} \{ \sqrt{n'} \delta_{n'-1,n} - \sqrt{n-1} \delta_{n'-1,n-2} \} \right. \\ &+ v_F \{ A_{n',s}^{+,p} B_{n,s}^{+,p'} \delta_{n'-1,n} - A_{n,s}^{+,p'} B_{n',s}^{+,p} \delta_{n',n-1} \} \end{aligned}$$

$$\left. + v_0 (\alpha - \beta) B_{n,s}^{+,p} B_{n',s}^{+,p'} \{ \sqrt{n+1} \delta_{n',n+1} - \sqrt{n'} \delta_{n',n-1} \} \right], \quad (35)$$

and for $\tau = -1$ and $n \geq 1$ as

$$\begin{aligned} & \langle n', s, -, p | \hat{v}_y | n, s, -, p' \rangle \\ &= (-i) \left[(\alpha + \beta) v_0 A_{n,s}^{-,p} A_{n',s}^{-,p'} [\sqrt{n'+1} \delta_{n',n+1} - \sqrt{n'} \delta_{n',n-1}] \right. \\ &+ v_F \{ A_{n',s}^{-,p} B_{n,s}^{-,p'} \delta_{n',n-1} - A_{n,s}^{-,p'} B_{n',s}^{-,p} \delta_{n-1,n} \} \\ &+ v_0 (\alpha - \beta) B_{n,s}^{-,p} B_{n',s}^{-,p'} [\sqrt{n} \delta_{n'-1,n} - \sqrt{n-1} \delta_{n'-1,n-2}] \end{aligned} \quad (36)$$

The velocity matrix elements corresponding to ground states for K-valley ($\tau = +1$) are

$$\begin{aligned} \langle 0, s, +, p | \hat{v}_y | n', s, +, p' \rangle &= A_{n',s}^{+,p'} v_F \delta_{0,n'-1} + v_0 B_{n',s}^{+,p'} (\alpha - \beta) \\ &\times [\sqrt{n'+1} \delta_{0,n'+1} + \sqrt{n'} \delta_{0,n'-1}] \end{aligned} \quad (37)$$

and

$$\begin{aligned} \langle n', s, +, p | \hat{v}_y | 0, s, +, p' \rangle &= (-i) [A_{n',s}^{+,p'} v_F \delta_{n'-1,0} \\ &+ v_0 B_{n',s}^{+,p'} (\alpha - \beta) \delta_{n',1}]. \end{aligned} \quad (38)$$

Similarly for K'-valley ($\tau = -1$)

$$\begin{aligned} \langle 0, s, -, p | \hat{v}_x | n', s, -, p' \rangle &= A_{n',s}^{+,p'} v_0 [\delta_{0,n'+1} + \sqrt{n'} \delta_{0,n'-1}] \\ &- v_F B_{n',s}^{+,p'} (\alpha - \beta) \delta_{0,n'-1} \end{aligned} \quad (39)$$

Note that velocity matrix elements are non-zero only for $n' = n \pm 1$.

* colin.nano@gmail.com

- 1 K. S. Novoselov, A. K. Geim, S. Morozov, D. Jiang, Y. Zhang, S. Dubonos, I. Grigorieva, and A. A. Firsov, *Science* 306, 666 (2004).
- 2 A. H. Castro Neto, F. Guinea, N. M. R. Peres, K. S. Novoselov, and A. K. Geim, *Rev. Mod. Phys.* 81, 109 (2009).
- 3 K. F. Mac, K. F. McGill, J. Park and P. L. McEuen, *Science* 344, 1489 (2014).
- 4 Z. Li and J. P. Carbotte, *Phys. Rev. B* 86, 205425 (2012).
- 5 M. Tahir, A. Manchon and U. Schwingenschlogl, *Phys. Rev. B* 90, 125438 (2014)
- 6 D. Xiao, G. Liu, W. Feng, X. Xu and W. Yao, *Phys. Rev. Lett.* 108, 196802 (2012)
- 7 K. F. Mak, C. Lee, J. Hone, J. Shan, and T. F. Heinz, *Phys. Rev. Lett.* 105, 136805 (2010);
- 8 A. Splendiani, L. Sun, Y. Zhang, T. Li, J. Kim, C. Y. Chim, G. Galli, and F. Wang, *Nano Lett.* 10, 1271 (2010);
- 9 T. Korn, D. Stich, R. Schulz, D. Schuh, W. Wegscheider, and C. Schuller, *Appl. Phys. Lett.* 99, 102109 (2011).
- 10 K. F. Mak, K. He, J. Shan, and T. F. Heinz, *Nat. Nanotechnol.* 7, 494 (2012)
- 11 H. Zeng, J. Dai, W. Yao, D. Xiao, and X. Cui, *Nat. Nanotechnol.* 7, 490 (2012)
- 12 B. Radisavljevic, A. Radenovic, J. Brivio, V. Giacometti, and A. Kis, *Nat. Nanotechnol.* 6, 147 (2011).

- 13 Jelena Klinovaja and Daniel Loss, *Phys. Rev. B* 88, 075404 (2013).
- 14 S. Wu, J. S. Ross, G.-B. Liu, G. Aivazian, A. Jones, Z. Fei, W. Zhu, D. Xiao, W. Yao, D. Cobden, and X. Xu, *Nat. Phys.* 9, 149 (2013).
- 15 V. P. Gusynin and S. G. Sharapov, *Phys. Rev. Lett.* 95, 146801 (2005).
- 16 M. Tahir and K. Sabeeh, *J. Phys.: Condens. Matter* 24, 135005 (2012).
- 17 P. M. Krstajic and P. Vasilopoulos, *Phys. Rev. B* 86, 115432 (2012).
- 18 Yuanbo Zhang, Yan-Wen Tan, Horst L. Stormer and Philip Kim, *Nature* 438, 201 (2005)
- 19 K. S. Novoselov, Z. Jiang, Y. Zhang, S. V. Morozov, H. L. Stormer, U. Zeitler, J. C. Maan, G. S. Boebinger, P. Kim, A. K. Geim, *Science* 315, 1389 (2007).
- 20 M. Tahir and U. Schwingenschlogl, *Sci. Rep.* 3, 1075 (2013).
- 21 Kh. Shakouri, P. Vasilopoulos, V. Vargiamidis, and F. M. Peeters, *Phys. Rev. B* 90, 235423 (2014).
- 22 X. Cui, G.-H. Lee, Y. D. Kim, G. Arefe, P. Y. Huang, C.-H. Lee, D. A. Chenet, X. Zhang, L. Wang, F. Ye, F. Pizzocchero, B. S. Jessen, K. Watanabe, T. Taniguchi, D. A. Muller, T. Low, P. Kim, and J. Hone, *Nat. Nanotechnol.* 10, 534 (2015)
- 23 M. Tahir, P. Vasilopoulos and F. M. Peeters, *Phys. Rev. B* 93, 035406 (2016).
- 24 Habib Rostami and Reja Asgari, *Phys. Rev. B* 91, 075433 (2015).

-
- ²⁵ Habib Rostami, Ali G. Moghaddam, and Reza Asgari, *Phys. Rev. B* 88, 085440 (2013).
- ²⁶ S. Lebegue and O. Eriksson, *Phys. Rev. B* 79, 115409 (2009).
- ²⁷ A. Kormanyos, V. Zolyomi, N. D. Drummond, P. Rakyta, G. Burkard, and V. I. Falko, *Phys. Rev. B* 88, 045416 (2013).
- ²⁸ Felix Rose, M. O. Goerbig, and Frederic Piechon, *Phys. Rev. B* 88, 125438 (2018).
- ²⁹ X. F. Wang and P. Vasilopoulos, *Phys. Rev. B* 67, 085313 (2003).
- ³⁰ Y. Zheng and T. Ando, *Phys. Rev. B* 65, 245420 (2002); T. Stauber, N. M. R. Peres, and F. Guinea, *ibid.* 76, 205423 (2007).
- ³¹ F. M. Peeters and P. Vasilopoulos, *Phys. Rev. B* 46, 4667 (1992).
- ³² M. Charbonneau, K. M. Van Vliet, and P. Vasilopoulos, *J. Math. Phys.* 23, 318 (1982).
- ³³ B. Radisavljevic and A. Kis, *Nat. Mater.* 12, 815 (2013).

This figure "mos2.png" is available in "png" format from:

<http://arxiv.org/ps/1604.05007v1>